Nano Energy 74 (2020) 104893

Contents lists available at ScienceDirect

Nano Energy

journal homepage: http://www.elsevier.com/locate/nanoen

Edge effect in silicon solar cells with dopant-free interdigitated back-contacts

Hao Lin [a,b], Jiajia Wang [c], Zilei Wang [b], Zhiyuan Xu [b], Pingqi Gao [b,*], Wenzhong Shen [a,*]

[a] Institute of Solar Energy, Key Laboratory of Artificial Structures and Quantum Control (Ministry of Education), School of Physics and Astronomy, Shanghai Jiao Tong University, 800 Dong Chuan Road, Shanghai, 200240, China
[b] School of Materials, Sun Yat-sen University, Guangzhou, 510275, China
[c] Ningbo Institute of Material Technology and Engineering, Chinese Academy of Sciences (CAS), Ningbo, 315201, China

ARTICLE INFO

Keywords:
Solar cells
Silicon heterojunction
Interdigitated back-contact
Carrier-selective contacts
Dopant-free
Edge recombination

ABSTRACT

Dopant-free heterojunction opens new doors to highly efficient silicon solar cells with interdigitated back-contacts (IBC) via an easy hard-mask processing. However, the existence of inevitable overlap between the hole- and electron-transport layers may cause edge leakage and recombination, which will deteriorate the power conversion efficiency. Here we unambiguously determined the edge recombination and recombination losses quantitatively, in combination with detailed comparisons in photovoltaic parameters, dark and light current-voltage (*I–V*) curves, partially illuminated *I–V* curves, of the hard-mask processed and the lithography processed IBC devices. Without the interfacial passivation layer, the solar cells fabricated by the hard-mask method suffer severe edge recombination with loss of 3×10^{-4} A and a quite poor fill factor (*FF*) of ~66%, suggesting that the edge recombination could be another important issue affecting the *FF* besides the series resistance. With the clear understanding of the edge effect, we finely control the edge overlap, and finally obtained silicon dopant-free solar cells (with of intrinsic amorphous silicon as passivation layer) with over 20% efficiency and 73% *FF* either by lithography or by hard-mask methods.

1. Introduction

The record power conversion efficiency (PCE) of single-junction crystalline silicon (c-Si) solar cells so far reaches 26.7% [1]. This device combines the interdigitated back-contact (IBC) structure with heterojunction of doped/intrinsic amorphous silicon (a-Si:H) [2,3], called IBC-silicon heterojunction (IBC-SHJ) solar cell. Because both the positive and negative electrodes are put on to the rear side of the solar cells, the electrode shading loss is completely eliminated and the parasitic absorption loss relating to the front doping layer is reduced. These two advanced aspects endorse an extremely high short circuit current density (J_{sc}). In addition, the IBC-SHJ cells also benefit from the excellent passivation quality provided by the intrinsic a-Si:H layer, and a promising open circuit voltage (V_{oc}) is thus ensured by the SHJ design. However, current studies on IBC-SHJ cells do stop at a laboratory scale because the developments towards large-scale industrial-level production are heavily limited by the complex fabrication process and the huge investment on facilities. The lack of cost-effective patterning method of the interdigitated electrode stacks is a primary constraint. In particular, the steps, including a-Si:H deposition and the subsequent patterning for isolations, during the fabrication of an IBC-SHJ cell, highly relies on expensive facilities including chemical vapor deposition, photolithography, dry etching, etc [4].

In this context, dopant-free heterojunction emerges as a hot topic as it can be deposited by simple methods, such as evaporation and spin-coating [5–7]. The formation of dopant-free heterojunctions relies on the work functions of the functional materials themselves, so additional doping is not required. This technology is a more cost-effective alternative to the conventionally doped a-Si:H. The carrier transport layers can be divided into hole transport layer (HTL) and electron transport layer (ETL) according to which type of carriers is transported. So far, one kind of the most successful HTL materials are transition metal oxides (TMOs), including molybdenum oxide (MoO_x) [8,9], vanadium oxide (VO_x) [10] and tungsten oxide (WO_x) [9], and all possess high work function property that benefits hole transportation. Oppositely, metal oxides like magnesium oxide (MgO_x) [11], titanium oxide (TiO_x) [12,13], salts like magnesium fluoride (MgF_x) [14], lithium fluoride (LiF_x) [15], are all low work function behavior and have small barrier offset

* Corresponding authors.
E-mail addresses: gaopq3@mail.sysu.edu.cn (P. Gao), wzshen@sjtu.edu.cn (W. Shen).

https://doi.org/10.1016/j.nanoen.2020.104893
Received 8 February 2020; Received in revised form 10 April 2020; Accepted 26 April 2020
Available online 11 May 2020

with the conduction band of n-Si, always serving as ETL materials. Furthermore, it is of great reference value for fabricating a novel IBC silicon solar cell with dopant-free heterojunction (we name it as IBC-DFHJ).

In 2016, Um et al. [16] used MoO_x and LiF_x as HTL and ETL, respectively, to prepare IBC-DFHJ solar cells with the efficiency of 15.4%. Compared to the traditional IBC-SHJ solar cells, the simple preparation process attracts great attention. For example, Wu et al. further simplified the method by using a hard-mask method instead of lithography and fabricated IBC-DFHJ solar cells [17]. They compared the performances of cells with different HTL materials of MoO_x, WO_x and V_2O_x, and finally obtained the best PCE of 16.6% from the device with V_2O_x/Si heterojunction. In 2017, Masmitja et al. [18] obtained a PCE of 19.1% by applying V_2O_x as HTL and Al_2O_3/TiO_2/Mg/Al as ETL in their IBC-DFHJ solar cells. In 2018, Wu et al. [19] successfully realized 22.2% PCE of IBC-DFHJ solar cells by adding a thin passivation layer of intrinsic a-Si:H in between the carrier transport layers (MoO_x as HTL and MgF_x as ETL) and the c-Si substrate. At the same time, our group reported IBC-DFHJ solar cells that were constructed by either solution-processed poly(3,4-ethylenedioxythiophene): polystyrene or evaporated metal oxides [20,21].

It is well known that, even for conventional front-back contacted solar cells, the edge quality of p-n junction will greatly affect the photovoltaic characteristics [22–24]. Because of the influence of edge recombination, the efficiency of silicon solar cells with a small area is often lower than that with a large area (a larger average distance from the edge region). In the IBC solar cells, the edge region of p-n junction is even longer in the interdigital structure of positive and negative electrodes. So the carrier recombination current at this region, caused by junction recombination, would largely reduce the PCE of IBC solar cells. Through the good suppression of this recombination, most of the devices would show obvious improvements in photovoltaic (PV) performance. For example, Muller et al. [25], found an increase in PCE of diffused-junction IBC cells by 2% absolutely after reducing the second-diode recombination current density (J_{02}) from 82 to 12 nA/cm^2.

Concerning the IBC-DFHJ solar cells, especially for the cells fabricated by hard-mask method, the relatively rough overlapping area between the HTL and ETL (naming gap region), may cause additional problems including edge leakage and recombination. In fact, unsatisfied fill factor (*FF*) has been found in our previous IBC-DFHJ solar cells fabricated by hard-mask method. Attributing the low *FF* straightforwardly to series resistance cannot well explain all experimental phenomena, as lower *FF*s were also shown in the IBC devices with extremely low contact resistance. The lack of study on the edge effect in IBC-DFHJ solar cells does not only restrict our understanding in the above phenomena, but also hinders us to improve the efficiency of this kind solar cells in future. Therefore, it is essential to quantitatively analyze the quality of edge region and study the influence of edge recombination (or edge effect) on the photovoltaic performance of IBC-DFHJ solar cells.

Here, we figured out the reason for low *FF* by comparing the IBC-DFHJ devices that were constructed by either hard-mask method or well-defined lithography technique. We quantitatively analyzed the recombination and determined the location of the recombination through a modified Cox and Strack method (CSM) and partial illumination method. It is shown that the lithography method with Al_2O_3 passivation layer at gap region suppresses the edge recombination well, making the recombination current (I_{0H}) below 5×10^{-10} A, while the I_{0H} reaches 3×10^{-4} A in the cells fabricated with a hard-mask method without gap passivation. The *FF* of the solar cells increases from ~66% of the hard-mask method to >75% of lithography method. This suggests that the edge recombination is another important issue affecting the *FF* besides the series resistance. According to above experimental data, we further proposed a simulation model and successfully explained the process of edge effect in hard-mask processed IBC-DFHJ devices. Based on the above understanding, we finally obtained IBC-DFHJ solar cells (with a-Si:H layer passivation layer) with over 20% efficiency and 73% fill factor by using both lithography and hard-mask methods.

2. Results and discussion

Fig. 1a–b shows the rear side photographs of the two types of IBC devices fabricated by hard-mask method and lithography method. The width of HTL, ETL and gap region are set as 1500 μm, 500 μm and 100 μm, respectively. Fig. 1c–d exhibit the corresponding cross-sectional schematic diagram of IBC-DFHJ solar cells with a pitch. Here, n-type silicon was selected as the substrate, random pyramid was used as the anti-reflection textures on the front surface, Al_2O_3 and SiN_x films were served as the passivation layer and anti-reflection layer, respectively. On the rear side of the solar cells, interdigitated MoO_x/Ag and LiF/Al were deposited to form the HTL and ETL, respectively. A 4-nm a-Si:H film would be inserted as passivation layer if required. The area between the HTL and ETL is called gap region, and the corresponding magnified schematics of this region are showed in Fig. 1e–f. As shown in Fig. 1e, the thickness of MoO_x film becomes thinner gradually at the edge, which is caused by the evaporation method with rotation. Note that the reason why we must apply this rotation method is to prevent the sequential Ag layer from directly contacting with silicon at the edge, which may generate a serious leakage channel. By contrast, the edge of MoO_x layer keeps the same thickness as other region and shows a distinct boundary line (Fig. 1f) in the situation of lithography method, because of the protection of photoresist. Using the hard-mask method, an ~10 μm wide transition region with Ag particle was observed in the SEM images, while it does not exist on such area in the sample fabricated by photolithography (Fig. S1). The corresponding light current density-voltage (*J-V*) curves and photovoltaic performance of the IBC-DFHJ solar cells produced by these two methods are shown in Fig. 1g and Table 1, respectively. The efficiency descent of the hard-mask processed device in comparison with the one fabricated by lithography could be mainly caused by the degraded *FF*. In the case of 0 nm a-Si:H, the *FF* decreased from 76.2% (lithography) to only 67.7% (hard-mask). The series resistances for both kinds of devices derived at open-circuit voltage (V_{oc}) point are almost the same and obviously cannot be a reasonable explanation for such a large difference in *FF*. Meanwhile, the difference of shunt resistance (R_{sh}) derived at J_{sc} point, decreased from the 5.8 kΩ cm^2 (lithography) to 0.7 kΩ cm^2 (hard-mask), indicating a possibly large leakage current at the p-n junction in the hard-mask processed IBC solar cell. However, from the further analysis of light *J-V* curve in Fig. S2, the real R_{sh} (representing the leakage current of p-n junction) of this hard-mask processed IBC-DFHJ solar cells is good enough, reaching at ~4 kΩ cm^2. This indicates that the low R_{sh} at J_{sc} is not caused by the leakage current of the p-n junction. When the passivation layer of 4 nm a-Si:H was introduced, the average PCE of lithography processed IBC solar cell approaches 20.2% (FF = 73.2%) while that of hard-mask method is still below 19% (*FF*<71%).

It is well known that a strong inversion layer forms when MoO_x layer contacts with n-type silicon, yielding a heterojunction that plays a similar role of p-n junction in conventional solar cells. The edge quality of such junction does greatly affect the photovoltaic characteristics, especially in the IBC-DFHJ structure, where the edge region of the heterojunction is longer than that of conventional one due to the interdigital structure of HTL and ETL. The edge recombination could be the main reason leading to the large *FF* loss in hard-mask processed IBC-DFHJ solar cells. Fig. 2 shows the edge recombination problem of IBC-DFHJ solar cells prepared by hard-mask method. Fig. 2a and b are the enlarged SEM image of the dotted black box in Figs. 1a and 2a, respectively. The inset in Fig. 2b shows the normalized profiles of the deposited MoO_x and Ag films. From Fig. 2b, it reveals that the thickness of MoO_x film becoming thinner gradually at the edge region, and the width of this gradient region is more than 120 μm (see the normalized contour lines of MoO_x film in the inset). To better understand the influence of edge recombination on the PV performance, an equivalent

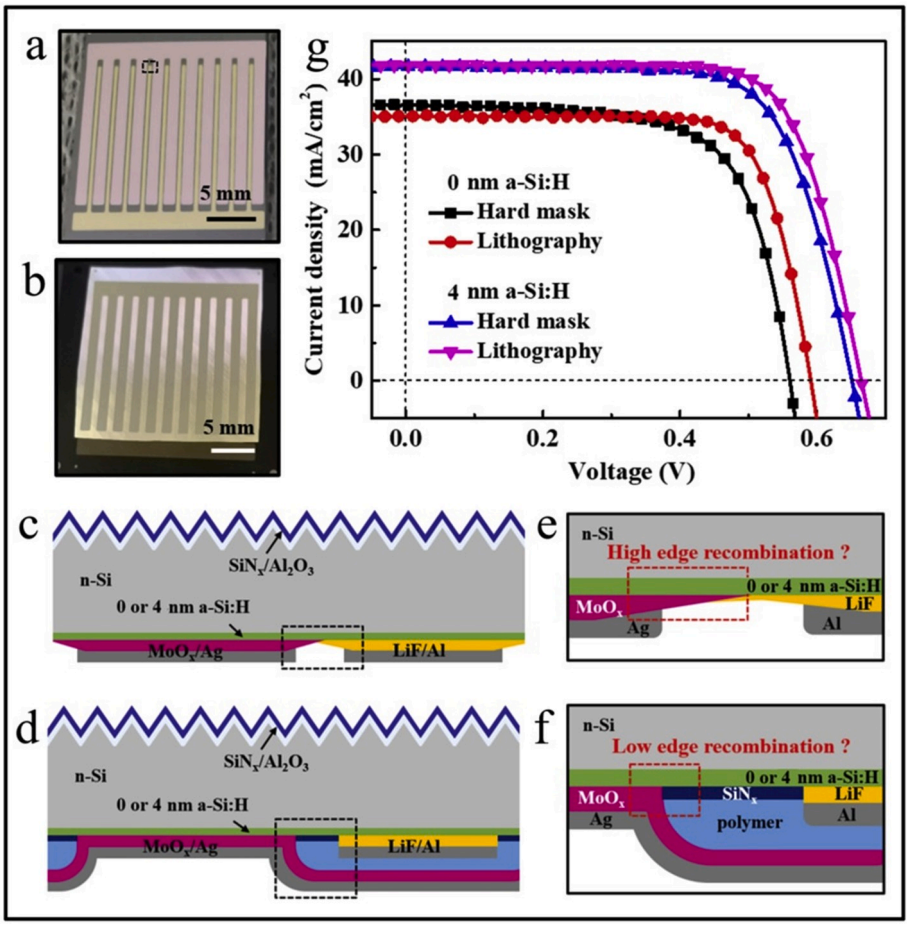

Fig. 1. Comparison of IBC-DFHJ solar cells fabricated by hard-mask method (a,c,e) and lithography method (b,d,f). (a,b) The photograph of the device's rear side. (c, d) The schematic diagram of solar cell structure. (e,f) The corresponding close-up of the gap region marked by black dashed boxes in (c) and (d), respectively. (g) The light *J-V* curves of IBC-DFHJ solar cells with 0 or 4 nm a-Si:H films.

Table 1
Photovoltaic performance of dopant-free IBC solar cells showed in Fig. 1g.

Thickness of a-Si:H[a]	Methods[a]	V_{oc}[b] (V)	J_{sc}[b] (mA/cm^2)	*FF*[b] (%)	PCE[b] (%)	R_s *at* V_{oc}[b] (Ω·cm^2)	R_{sh} *at* J_{sc}[b] (kΩ·cm^2)
0 nm	**Hard mask**	**0.560** (0.558 ± 0.005)	**36.5** (36.2 ± 0.4)	**67.7** (65.7 ± 2.4)	**13.8** (13.5 ± 0.2)	**1.6** (1.7 ± 0.1)	**0.7** (0.8 ± 0.6)
	Lithography	**0.591** (0.584 ± 0.008)	**35.4** (34.8 ± 0.8)	**76.2** (75.5 ± 0.9)	**15.9** (15.2 ± 0.7)	**1.4** (1.6 ± 0.2)	**5.8** (4.2 ± 1.2)
4 nm	**Hard mask**	**0.651** (0.643 ± 0.011)	**41.6** (41.3 ± 0.3)	**70.8** (70.7 ± 1.1)	**19.2** (18.8 ± 0.6)	**2.1** (2.1 ± 0.2)	**3.1** (1.8 ± 0.9)
	Lithography	**0.666** (0.662 ± 0.006)	**41.6** (41.5 ± 0.3)	**73.2** (73.3 ± 0.7)	**20.3** (20.2 ± 0.2)	**2.4** (2.5 ± 0.3)	**21.3** (24.2 ± 15.3)

[a] Data and statistics based on five cells of each condition.
[b] Numbers in bold are the champion values of each condition.

circuit and the corresponding *J-V* curves of the solar cells with and without edge recombination are given in Fig. 2c and d. In the equivalent circuit, the dotted red box marked as H presents the high recombination contribution caused by edge effect. The distance from the edge to the collection electrode, leads to a resistance term, R_{0H}. Therefore, it includes the high recombination current density (J_{0H}) and R_{0H} [26–29]. After the introduction of serious edge recombination (Fig. 2d, parameters are showed in the inset), although both solar cells have the nearly same V_{oc} and J_{sc}, the filling factors of the solar cells are greatly reduced from the original ~72% to below 66%. The conversion efficiency of the solar cells was thus greatly reduced. More importantly, this curve well coincides with the experimental data in Fig. S2, in which the R_{sh} at J_{sc} is apparently smaller than the real R_{sh} (extracted by the slope of the *J-V* curves at negative bias of -0.6~-0.4 V).

We exhibited the edge recombination and calculated the *J-V* curves based on the assumed parameters of J_{0H} and R_{0H} (Fig. 2). Unfortunately, there are no available methods to extract the value of edge recombination experimentally for this newly developed IBC-DFHJ solar cell. Here, a traditional measuring method, Cox and Strack method (CSM), which is commonly used to measure the contact resistance [30,31], was modified by us to make it suitable for extraction of the edge recombination of MoO_x/n-Si heterojunction. Fig. 3a shows the schematic testing configuration of devices for edge recombination. The MoO_x and Ag thin films were deposited on the n-Si wafer to form disk-like MoO_x/n-Si

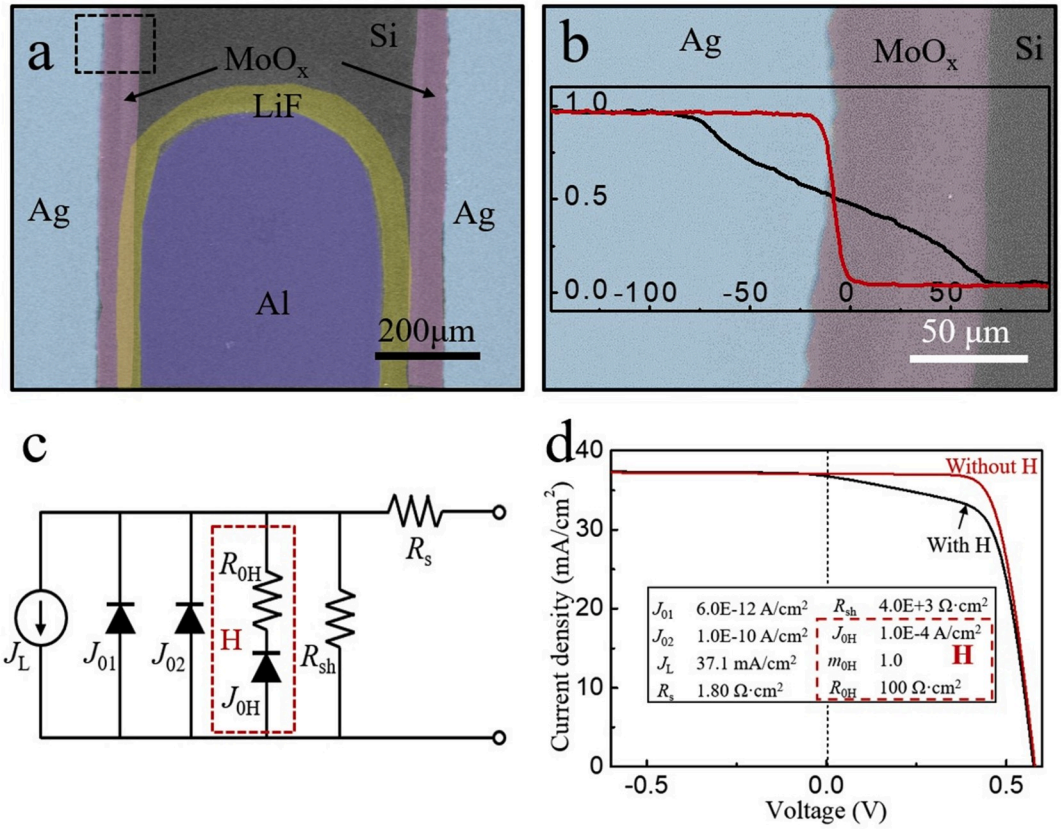

Fig. 2. Effect of edge recombination in IBC-DFHJ solar cells. (a) Amplified SEM image of black dashed boxes in Figure (a). (b) Amplified SEM image of black dashed boxes in (a). The inset is the normalized contour lines of Ag (red line) and MoO_x (black line) films. (c) The equivalent circuit for normal solar cells considering high recombination loss. (d) Illumination *J-V* curves of devices with and without high recombination loss (H). The inset is the table of simulation parameter.

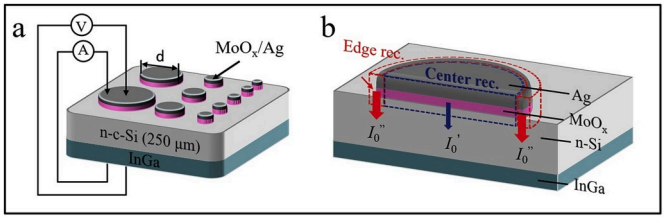

Fig. 3. Measuring method for the edge recombination of dopant-free heterojunction. (a) Schematic diagram of the test method. (b) The principle diagrams of measuring edge recombination.

heterojunctions with various diameters. With the measurement of *I–V* curves of those disks, the edge recombination can be defined through the analysis of experimental data. Fig. 3b shows the schematics of the amplified disk for analyzing the components of recombination current, which includes center recombination current (I_0') and edge recombination current (I_0''). Obviously, the center recombination current should be linearly proportional to the area of disk, while the edge recombination current should be linearly related to the perimeter of the disks [32–34]. Therefore, the $I_0 = I_0' + I_0''$ (1) can be written as

$$(\pi \cdot d^2/4) \cdot J_0 = (\pi \cdot d^2/4) \cdot J_0' + (\pi \cdot d) \cdot J_0'' \quad (2)$$

and after dividing $(\pi \cdot d^2/4)$ at both sides of equation, we can get $J_0 = J_0' + (4/d) \cdot J_0''$ (3), where the I_0 is total recombination current, J represents the current density and d is the diameter of the disks. According to the equation (3), we can easily quantify the edge recombination by changing the diameter of disks.

With this method, we began to measure the edge recombination of MoO_x/n-Si heterojunction. Fig. 4a shows the schematic of test structure fabricated by hard-mask method and lithography method, respectively. Al_2O_3 was introduced as passivation layer at the edge region in lithography method, and therefore it can be used for the comparison of the edge recombination of MoO_x/n-Si heterojunction with and without passivation in edge region. More details on the fabrication of testing samples are given in the experiment part. Fig. 4b presents the dark *I–V* characteristics of above two types of samples with three different diameters, 0.24, 0.12 and 0.06 mm. The data is plotted in three ways, current/area vs voltage (*J-V*), current/perimeter vs voltage (*I/P–V*) and local ideality factor vs voltage (*m-V*). When the voltage is lower than 0.35 V (Fig. 4b), the *I/P–V* curves of three diameters overlapped together, which represents a linear relationship between the recombination current and the perimeter. The ideality factor $m = \sim 2$ was derived around 0.3 V according to the linear dependence of recombination current on the $\exp(V/2V_T)$ in Exp.1, where V_T is the thermal voltage. In contrast, $m = \sim 1.3$ in Exp.2. It's well known that, the closer of the m value to 1, the more ideal of the junction is. Oppositely, it represents a high recombination in depletion-region when the value of m is closer to 2. It plotted the J_{01} ($m = 1$), J_{0H} ($m = m_{0H}$), and $1/R_{sh}$ as a function of 4/d in Fig. 4c, d, and e, respectively, and according to the equation (3), the recombination or shunt resistance from edge region can be extracted from the slope of the fitting line in Fig. 4c–e. Apparently, with the help of passivation at the edge region, the edge recombination and current leakage can be well suppressed, with J_{01}'' decreasing from 65 fA/cm to 3.8 fA/cm, J_{0H}'' decreasing from 3.8 nA/cm to 5.7 pA/cm, and R_{sh}'' increasing from 3.4×10^8 Ω·cm to 7.6×10^9 Ω cm. According to above date, the recombination current (I_{0H}'') from the edge region can be easily calculated. For an example, in the IBC-DFHJ solar cells fabricated by hard-mask method, the I_{0H} can reach $\sim 2 \times 10^{-7}$ A (3.8 nA/cm × 44 cm, where 44 cm is the perimeter of MoO_x/n-Si

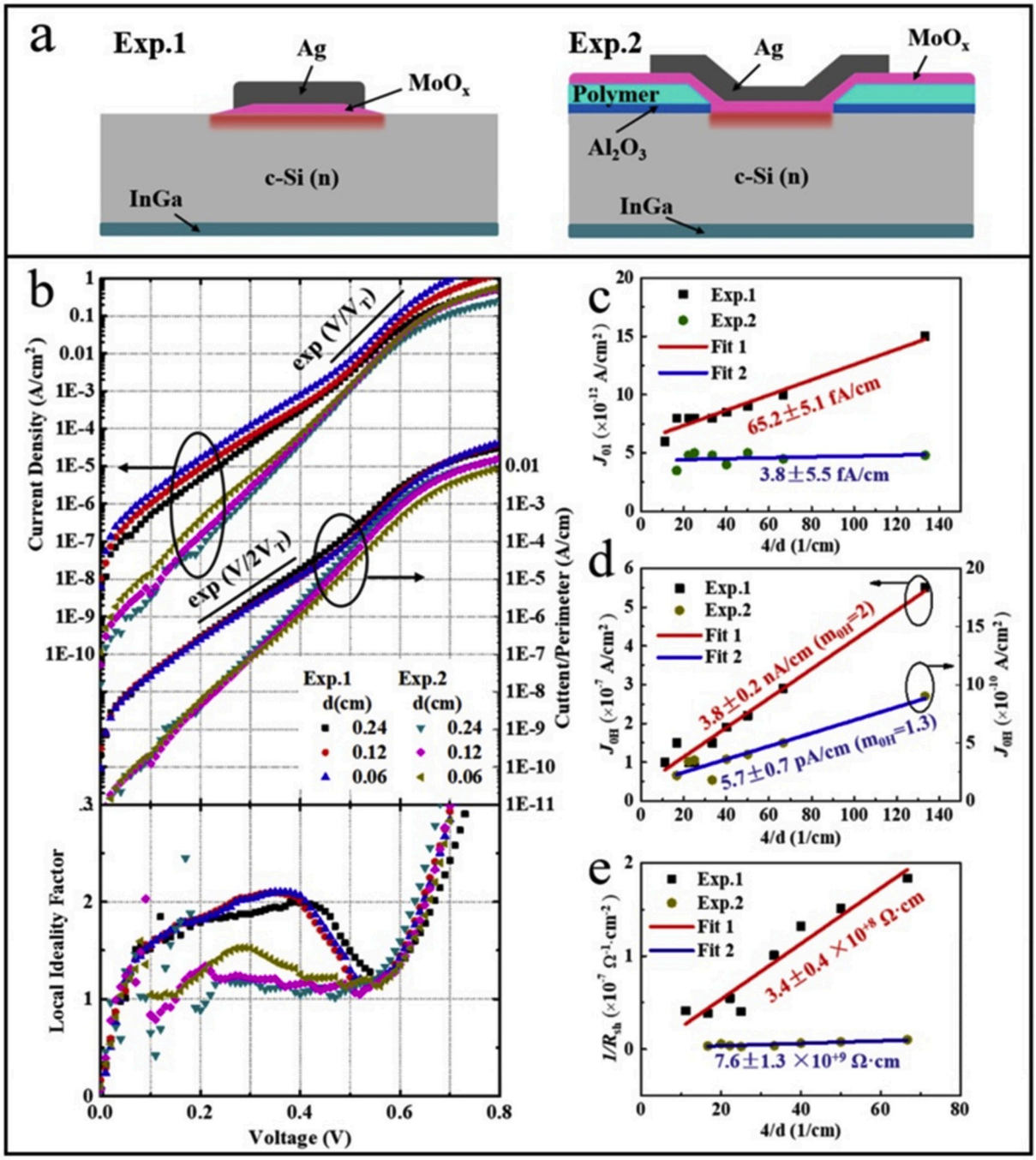

Fig. 4. Analysis of measuring results using the method in Fig. 3. (a) Schematic of test structure fabricated by hard-mask method (Exp.1) and lithography method (Exp.2). (b) *J-V*, *I/P–V* and *m-V* curves for the test structure in Figure (a). (c–e) Calculations of J_0" (c), J_{0H}" (d) and R_{sh}" (e) contributed by edge region.

heterojunction in the real IBC solar cells showed in Fig. 1a).

Above quantitative study only under dark condition is still not enough to fully reflect the edge effect because of the possible difference of recombination in dark and light conditions [35], therefore, *I–V* curves of IBC-DFHJ solar cells both in dark and light conditions are measured and analyzed in Fig. 5. The experimental data of dark *I–V* curve (and light *I–V* curve shifted by the short-circuit current I_{sc} [34,35]) are plotted in Fig. 5a and b, and the corresponding analysis *I–V* curves according to the equivalent circuit showed in Fig. 2c (includes R_{sh}, I_{01}, I_{02} and I_{0H}), are plotted by solid line. The quality of junction was reflected by *m-V* curves (Fig. 5c), which can be used to extract the parameters of the equivalent circuit. After well fitting, the parameters are extracted and listed in Table S1. For the main recombination items in dark *I–V*, I_{02} = 3.2×10^{-7} A, is well consistent with the value of I_{0H} (~2×10^{-7} A) evaluated in Fig. 4. It should be mentioned that, when $m_{0H} = 2$ and $R_{0H} = 0$ Ω, I_{0H} is equal to I_{02}. Therefore, it may difficult to distinguish the items of I_{02} and I_{0H}, especially when m_{0H} = ~2 and R_{0H} = ~0 Ω, but both of them can be recognized together as the recombination in p-n junction. From the comparison of the dark and light conditions, it is obvious that I_{0H} increased by nearly 6 orders of magnitude, from 5E-10 A to 3E-4 A (Table S1), and it has a distinctive hump in the *m-V* curve (Fig. 5c), which indicates a huge resistance limited enhanced recombination (very likely from edge recombination) will occur in light condition. This means that it suffers a more recombination in light compared with that in dark. Fig. 5d shows the experimental and fitting light *J-V* curves, where Fit 1 and Fit 2 are according to the results from dark *I–V* and light

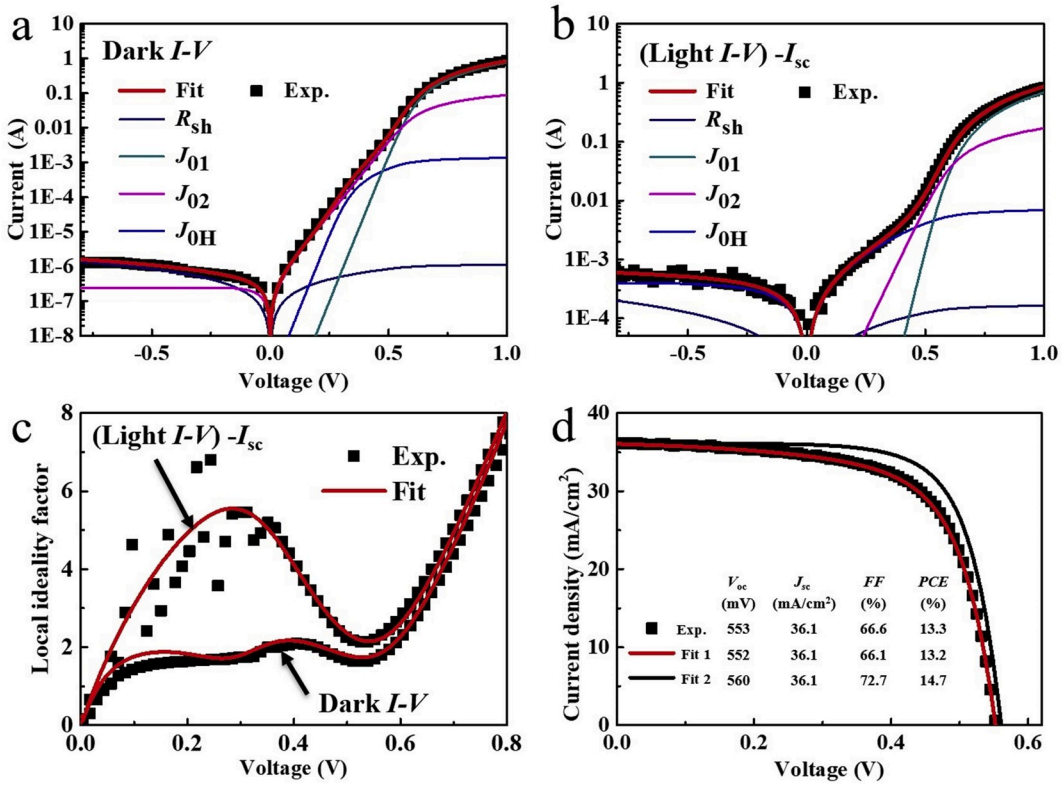

Fig. 5. Analysis of recombination difference between dark and light conditions in IBC-DFHJ device. (a) Analysis of Dark *I–V* curves. (b) Analysis of Light *I–V* curves. (c) Corresponding *m-V* curves extracted from Figure (a) and (b). (d) Experimental and fitting light *J-V* curves, where Fit 1 and Fit 2 are according to the results from Figure (a) and (b), respectively. Here, the IBC-DFHJ solar cell is fabricated by hard-mask method.

I–V curves, respectively. Compared to the situation in dark condition, an additional recombination item in light lead to even worse *FF*, with decreasing from ~73% in dark (Fit 2) to ~66% in light (Fit 1).

To figure out the approximate position of this additional recombination from, we further developed an analytical method based on local illumination. The details of the method are schematically shown in Fig. 6a. The measurement of IBC-DFHJ device under All, ETL and HTL area illuminations are achieved through using a special opaque mask. For convenience, we named above measurements as "All", "ETL" and "HTL", respectively. Here, for a fair comparison, we keep the total illumination area of above measurements as large as possible, and the actual total illumination area of "All", "ETL" and "HTL" are 1.0 cm^2, 0.81 cm^2 and 0.81 cm^2, respectively. Fig. 6b shows the light *I–V* curves shifted by the corresponding I_{sc} as well as the dark *I–V* curve, while the corresponding light *J-V* curves as well as *m-V* curves are shown in Fig. S3. The corresponding photovoltaic performances are listed in Table S2. One can see that the *I–V* curve of "HTL" is close to that of "Dark", while that of "ETL" nearly overlaps with that of "All". This result proves that the additional recombination mainly affects the collection of the photon-generated carriers on the ETL region. Because the excess minority carriers above the ETL region are mainly collected at the edge of HTL as current, it indicates the additional recombination is most likely from the edge region of HTL. After carefully fitting the *I–V* curves, we also extracted the value of equivalent circuit parameters, which has been listed in Table S1. Fig. 6c shows the calculated *FF* loss according to above extracted values (the other PV performance are listed in Table S2). From that, compared with the *FF* of "Dark", the *FF* for both "All" and "ETL" decrease to ~66% and ~60%, respectively. While that in "HTL" is nearly the same as the "Dark", at ~71%. It also shows that the *FF* loss caused by recombination is occupied the most proportion in all situations. That indicates the main reason of poor *FF* of this IBC-DFHJ solar cell does relate to the edge recombination.

Local illumination analysis was further applied to study the IBC-DFHJ solar cells fabricated by lithography method. As shown in Fig. 6d and Fig. S3d (the corresponding PV performance are listed in Table S2), all *I–V* curves or *m-V* curves nearly overlapped together, which indicates the superposition principle is suitable for the IBC devices fabricated by lithography method, and no additional recombination happens in light condition [36]. At the same time, the extracted parameters listed in Table S1 indicate a small recombination value in this structure, echoed by the suppressed I_{0H} of only 5.0E-10 A (m_{0H} = ~1.3). Finally, as shown in Fig. 6e, all tests reveal quite good *FF* beyond 75%.

Except for the difference of passivation layer at the gap region, the extending of the MoO_x in gap region is another obvious character in the IBC-DFHJ device fabricated by mask method. Therefore, IBC-DFHJ models with and without emitter (HTL) in the gap region are utilized to simulate the solar cells fabricated by the two methods (Fig. 7a). To reflect the actual conditions, the sheet resistance of emitter in gap region is set as 10^4 Ω/□, which is derived from the measurement of sheet resistance of inversion layer through using a transfer length method (TLM) [37]. As shown in Fig. 7b, with the growth of S_{gap} (the surface recombination rate of gap region), the *FF* in IBC-DFHJ model with emitter decreases quickly from >80% to <45%, while the *FF* for the one without emitter shows unchanged value at ~80%. Two conclusions can be drawn: (1) the MoO_x layer extended to the gap region increase the edge recombination, leading to the decrease of *FF*; (2) the recombination in the none-collection region (gap and ETL region) have negligible effect on the *FF* of IBC-DFHJ devices. From the transportation of holes in IBC-DFHJ devices (Fig. 7c), it shows the holes generated above the HTL will directly transmit to HTL, while that above the ETL will transmit across the gap, leading to the highest hole current density at the region of HTL. For the sample with MoO_x in gap (with emitter), this high hole current occurred at the middle of gap region will cause severe recombination. Finally, as shown in Fig. S4, with the help of a 2-nm passivation film of a-Si:H, IBC-DFHJ solar cells with efficiency up to 20.6% was

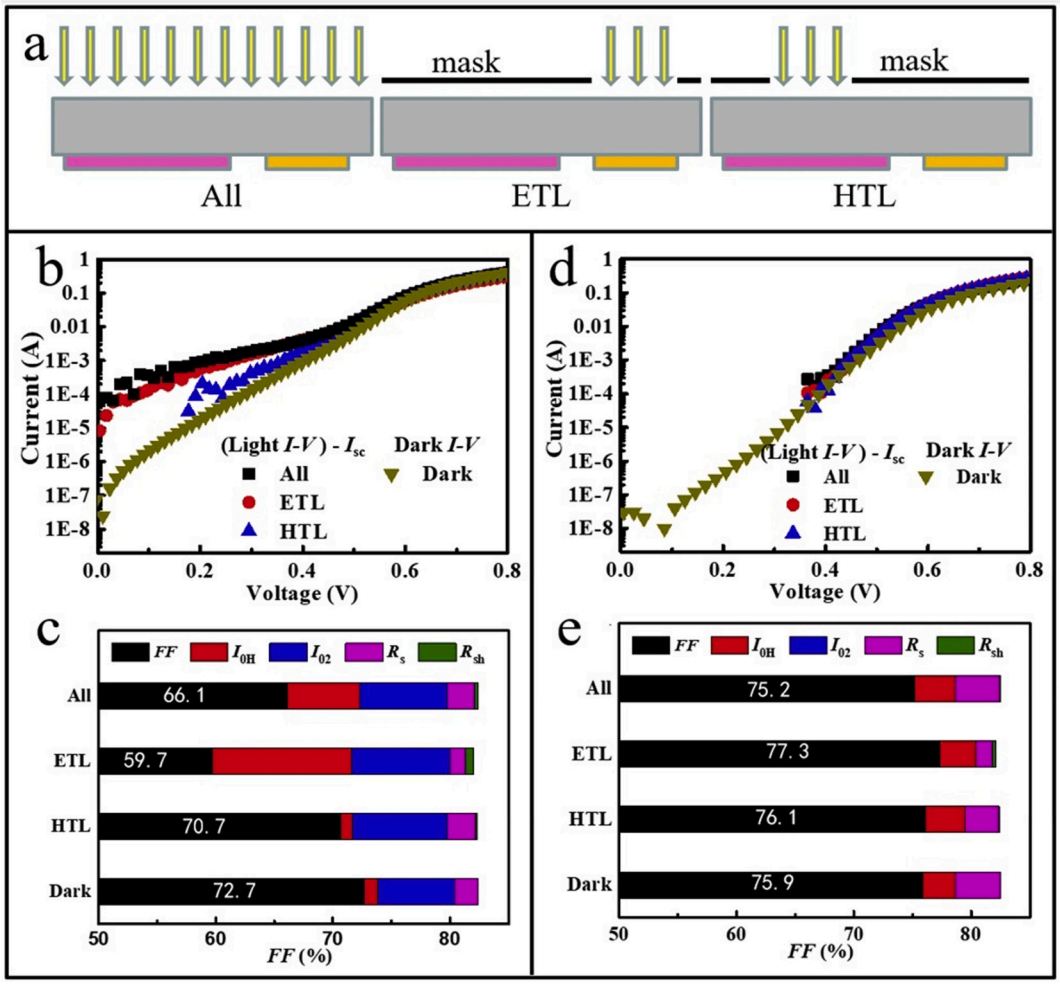

Fig. 6. Identification of high recombination region in IBC-DFHJ device fabricated by hard-mask method (b,c) and the comparison with that fabricated by lithography method (d,e). (a) Schematics of illumination test with different regions. (b,d) (light *I–V*)-I_{sc} and dark *I–V* curves for the different regions' illumination test in (a). (c,e) Analysis of *FF* loss.

achieved.

3. Conclusion

In this work, we systematically studied the edge recombination in silicon-based IBC solar cells with dopant-free heterojunction. Firstly, a modified Cox and Strack method (CSM) was proposed to extract the edge recombination loss of MoO_x/Si heterojunction. The results underline that the test device fabricated by hard-mask method reveals obvious higher edge recombination current density than that by lithography method, with decreasing J_{0H}" from 3.8 nA/cm to 5.7 pA/cm. Secondly, the *I–V* curves of IBC-DFHJ solar cells fabricated by hard-mask method was tested both in dark and light conditions. It exhibits an additional recombination channel in light condition in comparison with the case in dark, which limits the *FF* below 66%. Thirdly, through using local illumination method, the additional recombination in light was found to be related to the edge region of HTL. Fourthly, through using simulation method, HTL extending to the gap region may be another reason for the deteriorated edge recombination, leading to an even worse *FF*. With the guidelines from the above insight, we finally fabricated IBC solar cells with dopant-free heterojunction reaching efficiency to 20.6% and *FF* to 75.6%.

3.1. Experimental section

3.1.1. IBC-DFHJ solar cells fabrication

One side polished n-type (1–3 Ω cm) silicon wafers with 250 μm thickness were used to fabricate IBC solar cells. Firstly, random-pyramid textures were fabricated by 80 °C mixed solutions with 2.5 wt% NaOH and 1.5 wt% isopropanol for 15 min. And to obtain one side pyramid-textured wafer for fabricating IBC-DFHJ solar cells, a homemade tool was used to protect the polished side of the wafers in textures process. Secondly, above one-side pyramid textured wafers and the original wafers were cleaned by standard Radio Corporation of America (RCA) cleaning processes, and then were disposed by 4 wt% HF to remove SiO_2 on the surface of the wafers. Thirdly, the passivation layer, Al_2O_3 (~15 nm), and the anti-reflection layer, SiN_x (~75 nm), were deposited by atomic layer deposited (ALD) and plasma-enhanced chemical vapor deposition (PECVD), respectively. To activate the passivation of Al_2O_3, the samples were annealed at 450 °C in N_2 atmosphere for 30 min. And then, for the IBC-DFHJ devices inserting intrinsic hydrogenated amorphous silicon (a-Si:H) as passivation layer at the rear side, 4 wt% HF was dipped on the polished side of above sample to remove the Al_2O_3, followed which a-Si:H films with 2–4 nm thickness were deposited by PECVD, and SiN_x film (~80 nm) also be deposited if it is used for fabricating IBC devices through lithography method. Fourthly, through using thermal evaporation with the hard-mask or lithography pattern, MoO_x/Ag (10/400 nm) and LiF/Al (0.5/400 nm) films were deposited

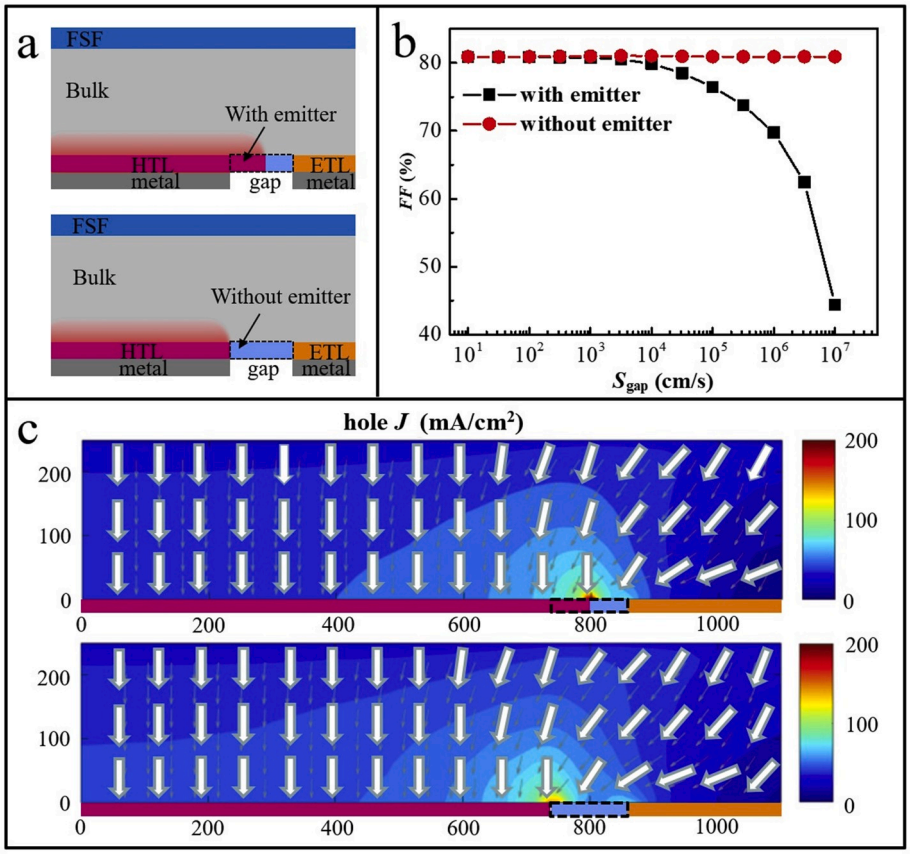

Fig. 7. Analysis of the possible reasons for *FF* loss in IBC-DFHJ device. (a) Schematics of IBC-DFHJ models with and without emitter (HTL) in the gap region. (b) Simulation results of *FF* as a function of S_{gap}. (c) Distribution of hole current density in IBC-DFHJ devices with and without emitter.

on the rear side as HTL and ETL, respectively, and more details about the preparation flow were showed in Fig. S5.

3.1.2. Fabrication of testing devices for extracting the edge recombination

One side polished n-type (1–3 Ω cm) silicon wafers with 250 μm thickness were used to fabricate these testing devices. In order to be consistent with the actual IBC-DFHJ solar cells, all wafers were cleaned by standard RCA cleaning processes, followed by a deposition of 15 nm Al_2O_3 film through ALD and 450 °C annealing in N_2 atmosphere. For the situation of using the lithography method, positive photoresist was spin-coated on the polished side of the wafers, and a hard-mask, containing an array of circular holes with different diameters, called C.S. mask 1, was used as photoresist mask. After exposure and develop, this array was transferred to the photoresist. Immersing the samples with photoresist pattern into 4 wt% HF solutions for 30s to remove the Al_2O_3 film of circular holes. Another hard mask, containing an array of circular holes with the same diameter (0.36 cm), called C.S. mask 2, was used to isolate each test pads. With the help of C.S. mask 2, an array of MoO_x/Ag (10 nm/400 nm) circular pads was formed by thermal evaporation. At last, InGa alloys was coated on the rear side of the test wafers by drawknife. For the situation of using the hard-mask method, the samples were directly immersed into 4 wt% HF solutions to remove the Al_2O_3 film, and the array of MoO_x/Ag (10 nm/400 nm) circular pads with different diameters were evaporated on the polished side of the testing wafers through using C.S. mask 1. And then, also, InGa alloys was coated on the rear side of the testing devices by drawknife.

3.1.3. Characterization

The morphological analysis of the samples was conducted by SEM (Hitachi S-4800). The *I–V* curves except for Light *I–V* curves were measured by a Keithley 4200-scs semiconductor parameter analyzer. The Light *I–V* curves of solar cells were measured under a simulated AM 1.5 spectrum sunlight illumination. The solar cells were shielded by an opaque mask with 1.0 cm^2 effective illumination area, except for the measurement of "HTL" and "ETL" in Fig. 6 (which were shielded by a special opaque mask showed in Fig. 6a). The EQE and reflectance spectra (350–1100 nm) were measured by a quantum efficiency measurement system (QEX10, PV Measurements). The minority carrier lifetime was measured by Sinton WCT-120 lifetime tester.

3.1.4. Simulation method

Quokka software was employed to simulate the photoelectric performances of IBC-SHJ solar cells. In device simulation, the main parameters were set as follows: The substrate was *n*-Si wafers with 3 ms bulk lifetime. The thickness of *n*-Si wafers was set as 250 μm, and the resistivity was chosen as 2 Ω cm. The surface recombination velocity of the front Al_2O_3/Si interface and ETL were set as 5 cm/s and 1000 cm/s, respectively, while the J_{01} of HTL was set as 5×10^{-12} A/cm^2. The dimensions of the devices' ETL, HTL and gap were 250 μm, 750 μm and 100 μm, respectively, where it only simulated the half-pitch of the IBC solar cells.

Declaration of competing interest

The authors declare that they have no known competing financial interests or personal relationships that could have appeared to influence the work reported in this paper.

CRediT authorship contribution statement

Hao Lin: Conceptualization, Methodology, Investigation, Software, Writing - original draft. **Jiajia Wang:** Investigation, Data curation. **Zilei**

Wang: Validation. **Zhiyuan Xu:** Resources. **Pingqi Gao:** Writing - review & editing, Visualization, Funding acquisition. **Wenzhong Shen:** Supervision, Funding acquisition.

Acknowledgments

This work was supported by the Major State Basic Research Development Program of China (2018YFB1500501, 2018YFB1500302), National Natural Science Foundation of China (61974168, 61674154, 11674225, 11834011, 11974242), Guangdong Basic and Applied Basic Research Foundation (2019B151502053), Zhejiang Provincial Natural Science Foundation (LR19E020001).

Appendix A. Supplementary data

Supplementary data to this article can be found online at https://doi.org/10.1016/j.nanoen.2020.104893.

References

[1] K. Yoshikawa, H. Kawasaki, W. Yoshida, T. Irie, K. Konishi, K. Nakano, T. Uto, D. Adachi, M. Kanematsu, H. Uzu, K. Yamamoto, Nat. Energy 2 (2017) 17032.
[2] S. De Wolf, A. Descoeudres, Z.C. Holman, C. Ballif, Green 2 (2012) 7–24.
[3] G. Lu, J. Wang, Z. Qian, W. Shen, Prog. Photovoltaics Res. Appl. 25 (2017) 441–451.
[4] A. Tomasi, B. Paviet-Salomon, Q. Jeangros, J. Haschke, G. Christmann, L. Barraud, A. Descoeudres, J.P. Seif, S. Nicolay, M. Despeisse, S. De Wolf, C. Ballif, Nat. Energy 2 (2017) 17062.
[5] C. Yu, S. Xu, J. Yao, S. Han, Crystals 8 (2018) 430.
[6] P. Gao, Z. Yang, J. He, J. Yu, P. Liu, J. Zhu, Z. Ge, J. Ye, Adv. Sci. 5 (2018) 1700547.
[7] Z. Wang, P. Li, Z. Liu, J. Fan, X. Qian, J. He, S. Peng, D. He, M. Li, P. Gao, Apl. Mater. 7 (2019), 110701.
[8] J. Bullock, A. Cuevas, T. Allen, C. Battaglia, Appl. Phys. Lett. 105 (2014) 232109.
[9] M. Bivour, J. Temmler, H. Steinkemper, M. Hermle, Sol. Energy Mater. Sol. Cell. 142 (2015) 34–41.
[10] L.G. Gerling, G. Masmitja, C. Voz, P. Ortega, J. Puigdollers, R. Alcubilla, Energy Procedia 92 (2016) 633–637.
[11] Y. Wan, C. Samundsett, J. Bullock, M. Hettick, T. Allen, D. Yan, J. Peng, Y. Wu, J. Cui, A. Javey, A. Cuevas, Adv Energy Mater 7 (2017), 1601863.
[12] X. Yang, Q. Bi, H. Ali, K. Davis, W.V. Schoenfeld, K. Weber, Adv. Mater. 28 (2016) 5891–5897.
[13] J. Cho, M. Debucquoy, M. Recaman Payo, S. Malik, M. Filipič, H.S. Radhakrishnan, T. Bearda, I. Gordon, J. Szlufcik, J. Poortmans, Energy Procedia 124 (2017) 842–850.
[14] Y. Wan, C. Samundsett, J. Bullock, T. Allen, M. Hettick, D. Yan, P. Zheng, X. Zhang, J. Cui, J. McKeon, A. Javey, A. Cuevas, ACS Appl. Mater. Interfaces 8 (2016) 14671–14677.
[15] J. Bullock, P. Zheng, Q. Jeangros, M. Tosun, M. Hettick, C.M. Sutter-Fella, Y. Wan, T. Allen, D. Yan, D. Macdonald, S. De Wolf, A. Hessler-Wyser, A. Cuevas, A. Javey, Adv Energy Mater 6 (2016), 1600241.
[16] H.D. Um, N. Kim, K. Lee, I. Hwang, J.H. Seo, K. Seo, Nano Lett. 16 (2016) 981–987.
[17] W. Wu, J. Bao, X. Jia, Z. Liu, L. Cai, B. Liu, J. Song, H. Shen, Phys. Status Solidi Rapid Res. Lett. 10 (2016) 662–667.
[18] Masmitjà G, Ortega P, Puigdollers J, Gerling L G, Martín I, Voz C and Alcubilla R J. Mater. Chem. 6 3977.
[19] W. Wu, W. Lin, S. Zhong, B. Paviet-Salomon, M. Despeisse, Z. Liang, M. Boccard, H. Shen, C. Ballif, in: AIP Conference Proceedings 040025, 2018.
[20] H. Lin, D. Ding, Z. Wang, L. Zhang, F. Wu, J. Yu, P. Gao, J. Ye, W. Shen, Nano Energy 50 (2018) 777–784.
[21] J. Wang, H. Lin, Z. Wang, W. Shen, J. Ye, P. Gao, Nano Energy 66 (2019) 104.
[22] P. Spinelli, B.W.H. van de Loo, A.H.G. Vlooswijk, W.M.M. Kessels, I. Cesar, IEEE J. Photovoltaics 7 (2017) 1176–1183.
[23] M.D. Abbott, J.E. Cotter, T. Trupke, R.A. Bardos, Appl. Phys. Lett. 88 (2006), 4346-181.
[24] K. Ruhle, M.K. Juhl, M.D. Abbott, L.M. Reindl, M. Kasemann, IEEE J. Photovoltaics 5 (2015) 1067–1073.
[25] R. Müller, C. Reichel, J. Schrof, M. Padilla, M. Selinger, I. Geisemeyer, J. Benick, M. Hermle, Sol. Energy Mater. Sol. Cell. 142 (2015) 54–59.
[26] C.M. Chong, S.R. Wenham, M.A. Green, Appl. Phys. Lett. 52 (1988) 407–409.
[27] C.B. Honsberg, S.R. Wenham, Prog. Photovoltaics Res. Appl. 3 (2007) 79–87.
[28] R. M K, C.B. Honsberg, in: Proc. 16th EC PVSEC, 2000.
[29] F. Hernando, R. Gutierrez, G. Bueno, F. Recart, V. Rodriguez, in: Proc. 15th EC PVSEC, Vienna, 1998, pp. 1321–1323.
[30] R.H. Cox, H. Strack, Solid State Electron. 10 (1967), 1213–8.
[31] W. Wang, H. Lin, Z. Yang, Z. Wang, J. Wang, L. Zhang, M. Liao, Y. Zeng, P. Gao, B. Yan, J. Ye, IEEE. J. Photovoltaics 9 (2019) 1113–1120.
[32] T.J. De Lyon, H.C. Casey, M.L. Timmons, J.A. Hutchby, D.H. Dietrich, Appli. Phys. Letts. 50 (1987) 1903–1905.
[33] A.M. Siade, C.B. Honsberg, S.R. Wenham, in: Proc. 28th IEEE PVSC, Anchorage, 2000, pp. 268–271.
[34] K.R. McIntosh, Lumps, Humps and Bumps: Three Detrimental Effects in the Current–Voltage Curve of Silicon Solar Cells, Centre for Photovoltaic Engineering: University of New South Wales, 2001.
[35] S.J. Robinson, A.G. Aberle, M.A. Green, J. Appl. Phys. 76 (1994) 7920–7930.
[36] F.A. Lindholm, J.G. Fossum, E.L. Burgess, IEEE Trans. Electron. Dev. 26 (1979) 165–171.
[37] G. Luis, S. Mahato, C. Voz, R. Alcubilla, J. Puigdollers, Appl. Sci. 5 (2015) 695–705.

Hao Lin received his B.S. and M.S. degree in faculty of Science from Ningbo University, China, in 2010 and 2013, respectively. From 2012 to 2015, he worked in department of Physics and Materials Science, City University of Hong Kong. He received his Ph.D. degree from Shanghai Jiao Tong University, in 2019. Currently, he is a postdoctor in Sun Yat-sen University. His research interests include the solar energy materials, antireflection structure and dopant-free all-back-contact solar cells.

Jiajia Wang received her B.S. degree in Materials Science and Engineering from Nanchang University, China, in 2017. She is currently working toward the M.S. degree with the Ningbo Institute of Materials Technology and Engineering, Chinese Academy of Science, China. Her research interests focus on dopant-free high efficiency Silicon heterojunction solar cells.

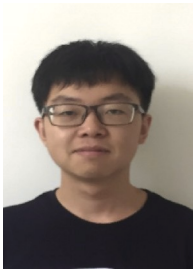

Zilei Wang received his B.S. degree in College of Physics and Information Engineering at Fuzhou University, China, in 2015. Currently, he is a Ph.D. candidate in Condensed Matter Physics at School of Physical Science and Technology at Lanzhou University. He is involved in a program at Sun Yat-sen University. His research interests focus on dopant-free silicon heterojunction solar cells.

Zhiyuan Xu is a M.S. candidate in Materials Engineering in School of Physical Science and Technology at Lanzhou University. He received his B.S. degree in College of Materials at Northwestern Polytechnical University in 2018. He is involved in a program at Sun Yat-sen University. His current research focuses on crystalline silicon/compound heterojunction.

Pingqi Gao received Ph.D. degrees in Department of Physics from Lanzhou University in 2010. From 2007 to 2011, he worked in Nanyang Technological University as a visiting researcher and a research staff. In 2013, he joined Ningbo Institute of Materials Technology and Engineering, CAS, as an associate professor and then a professor (2015). He joined Sun Yat-sen University in 2018. His research focus on high efficiency solar cell technology, especially on developing new materials and processes for solar energy conversion. He has published over 120 journal papers and serves as an active referee for 20 journals.

Wenzhong Shen received his Ph.D. degree in semiconductor physics and semiconductor device from Shanghai Institute of Technical Physics, Chinese Academy of Sciences, in 1995. Since 1999, Dr. Shen has been with Shanghai Jiao Tong University, China, as a full professor in the School of Physics and Astronomy, where he is currently the director of Institute of Solar Energy and Key Laboratory of Artificial Structures and Quantum Control, Ministry of Education.